Assessment of heat transfer measurements at drop/wall interactions: relation with the impact conditions

A. S. Moita[*1], A. L. N. Moreira[1]
[*1]Center for Innovation, Technology and Policy Research – IN+
Instituto Superior Técnico. Av. Rovisco Pais, 1049-001 Lisbon, Portugal

Abstract

The study presented here addresses the heat transfer mechanisms occurring at droplet/wall interactions. The experiments encompass the measurement of the instantaneous surface temperatures and the evaluation of the heat flux between the liquid and the surface, within a wide range of impact conditions. The results stress a strong dependence of the cooling performance of the droplets with the liquid and solid thermal effusivities rather than with other parameters, such as droplet diameter and impact velocity. So, the cooling performance of the impinging droplets, determined from the experimental results can be well described in the dimensionless space Prandtl-Weber numbers.

Introduction

The accurate description of the heat transfer mechanisms occurring at droplet/wall interactions is vital in cooling systems based on droplet [1] or spray [2] impact. Some common applications exploring the potential of such systems include the metallurgy and electronics industry (*e.g.* [3, 4]), although increasing interest is observed in a variety of other applications, from industrial safety in nuclear power plants to solar cells [5].

In these applications it is important to have a good indication of the instantaneous surface temperatures at different working conditions. For instance, many authors (*e.g.* [6]) have clearly shown the potential of spray cooling systems working near the CHF temperature, to take advantage of the additional parcel of the latent heat of evaporation, but care must be taken to avoid hot spots, which will lead to the sudden temperature increase and ultimately may result in system burnout. Nevertheless, studies reporting instantaneous measurements of surface and/or droplet temperature are quite scarce in the literature *(e.g.* Tartarini *et al.* [7]), particularly for impinging droplets ([8-11].

On the other hand, it is also essential to assess the heat transferred for different impact conditions in order to optimize the cooling performance of the system at given working condition. These systematic studies are also required to establish practical correlations, (usually as a function of the Weber, the Reynolds, the Jakob and the Prandtl numbers), within the various heat transfer regimes, which often provide the foundation for more complex formulations concerning spray impact (*e.g.* [12]).

This is the aim of the present paper, which addresses the study of the heat transfer mechanisms occurring between single droplets of several liquids and a variety of solid surfaces, made of diverse materials, within a broad range of impact conditions. This procedure allowed concluding on the role of the various factors governing the heat transfer mechanisms and, consequently on the parameters which can be used to optimize the cooling performance of the impinging droplets.

Materials and Methods

The experiments addressed here concern the impact on individual droplets onto solid, dry surfaces which are accommodated on a copper base in which a 264 W cartridge heater is inserted.

The surfaces are heated from room temperature up to 310ºC to cover the entire range of heat transfer regimes, from single phase evaporation to film boiling. The heat transfer regimes are identified based on the measurement and evaluation of the surface and contact temperatures during droplet/surface interaction, complemented with visual inspection of the morphology of the spreading lamella. Moreover, the critical heat flux (T_{CHF}) and, particularly the Leidenfrost temperatures ($T_{Leidenfrost}$) are evaluated for dynamic conditions (U0≠0), given their dependence on the properties of the system (surface properties and impact conditions).

Care is taken to assure that the surface is dry and recovers the initial temperature before the impact of the droplet. The liquid is kept at the droplet generator at room temperature and atmospheric pressure. Ambient tem-

* Corresponding author: anamoita@dem.ist.utl.pt

perature and relative humidity were measured through the experiments to ensure that their variation did not produce relevant changes in the results.

Although the rig allows varying the impaction angle, the present study focuses only on droplet impacts normal to the surface.

Several liquids (water, ethanol and methoxy-nonafluorobutane - $C_4F_9OCH_3$, usually called HFE7100) were selected to test a wide range of effusivities and thermo-physical properties. In line with this, the impact conditions are varied to cover a broad range of the most relevant dimensionless groups, (65<Weber number $We = \rho D_0 U_0^2 / \sigma_{lv}$ <1314; 170<Reynolds number $Re = U_0 D_0 / \nu$<11140; 2<Prandtl number $Pr = \nu C_p \rho / k$ <20, and 0.1<Jakob number $Ja = C_p (T_w - T_{sat}) / h_{fg}$ <1.9), which address the relative magnitude of the forces acting on the droplet. Here, *We* and *Re* are based on the drop initial diameter and impact velocity. T_w and T_{sat} are the surface temperature and the saturation temperature of the liquid, respectively, C_p is the specific heat and h_{fg} is the latent heat of evaporation. σ_{lv} and ν stand for the liquid surface tension and kinematic viscosity, respectively.

The working conditions are summarized in Table 1, while Table 2 depicts the thermo-physical properties of the liquids. These reference values taken at 25ºC, as well as their variation with temperature are obtained from Incropera [13], Özisik [14], Turns [15] and from the 3M Database for the HFE7100.

Table 1. Experimental conditions.

Liquid	D_0 [mm]	U_0 [ms^{-1}]	$T_{w,0}$ [ºC]
Water	2.8-3.0	0.4-3.1	25-310
Ethanol	2.2-2.4	0.4-2.5	25-260
HFE7100	1.7-2.0	0.4-2.5	25-260

Table 2. Thermophysical properties of the liquids. [a]From Tamura and Tanasawa [17]. [b]From Qiao and Chandra [18].

Properties	Water	Ethanol	HFE7100
Surface tension [Nm^{-1}]x10^3	73.75	22.0	13.6
Specific mass [kgm^{-3}]	998	790	1430
Kinematic viscosity [m^2s^{-1}]x10^6	1.0	1.4	0.38
Specific heat [$KJkgK^{-1}$]	4.18	2.44	1.18
Thermal conductivity [$Wm^{-1}K^{-1}$]x10^3	607.1	169	68.8
Latent heat of evaporation [$KJKg^{-1}$]	2272	846	122.6
T_{sat} [ºC]	100	78.3	61.0
$T_{Leidenfrost}$ [ºC] (nominal)	230[b]	182[a]	140

Droplet impact is recorded by two synchronized high-speed cameras (a Kodak Motion Corder Analyzer, Series SR 512x420pixels, Model PS-120, with a maximum frame rate of 10kfps and a Phantom v4.2 from Vision Research Inc., with 512x512pixels@2100fps and a maximum frame rate of 90kfps), as in Moita and Moreira [16], to provide both side and bottom view images of the spreading lamella.

The surface temperature of the targets is monitored by thermocouples type K and managed by a PMA KS20-I temperature controller. One of the thermocouples is a fast response "Medtherm" eroding-K-type which is embedded at the centre of the region where droplets impact. The signal of the thermocouples is sampled with a National Instruments DAQ board plus a BNC2120 and amplified with a gain of 300 before processing.

All the instrumentation is triggered by the same signal, emitted as the drop crosses a horizontal laser beam aligned with a photodiode.

Transparent smooth glass surfaces heated by Joule effect from the back side with a transparent film of Indium Oxide, In_2O_3 were used to visualize the liquid-solid interface. The temperature of these targets is monitored by contact thermocouples of type K, which are positioned over the glass side. Given that, in this case, the thermocouples could not be embedded in the surface, beneath the droplet, the contact temperature as defined by Seki *et al.* [19] was considered for comparative purposes.

Deposition of the film is made by radio frequency (rf) plasma enhanced reactive thermal evaporation (rf-PERTE) at low substrate temperature (<100^{o}C). Details of the method and of the resulting relevant film properties are reported by Carvalho *et al.* [20]. This deposition process allows obtaining a homogeneous film along the surface, as confirmed by scanning electron microscopy with x-ray microanalysis (SEM/EDS).

Characterization of the surfaces

The surfaces used in the present study are made of stainless steel AISI316, with thermal effusivity, ε_w of $7.2 \cdot 10^3 kg/Ks^{2.5}$.

The characterization of the surface topography naturally plays a crucial role. The amplitude of the rough peaks is quantified by the mean roughness, R_a, determined according to standard BS 1134 and by mean peak-to-valley roughness, R_z calculated according to standard DIN4768. The measurements are performed with an optical profile meter, (Surface Measuring System RM600-3D) which allows the 3D reconstitution of the surface topography. The main topographical characteristics of the targets are shown in Table 3.

Each pair liquid-surface is also characterized by the equilibrium contact angles, θ, which were measured at room temperatures, inside a thermostatted ambient chamber (Ramé-Hart Inc., USA, model 100-07-00), using the Sessile Drop Method. For water drops deposited on the smooth stainless steel surfaces, θ_1=93.0º and θ_2=93.5º, while for the smooth glass surface ($R_a \approx 0 \mu m$) used for visualization purposes, the contact angle with water is θ_4=38.5º. Complete wetting ($\theta \approx 0º$) is observed for all the surfaces when wetted by the ethanol and by the HFE7100 droplets.

A detailed description of the measurement procedures is presented in Moita and Moreira [21].

Table 3. Main topographical characteristics of the target surfaces.

Surface number	Surface Material	R_a [μm] ±10%	R_z [μm]
1	Stainless steel	0.31	2.32
2	Stainless steel	0.52	9.0
3	Glass	≈0	≈0

Results and Discussion

The dynamic behaviour of a droplet impacting onto a solid and heated surface is well known to depend on the heat transfer regime. While T_{w0} remains below the saturation temperature of the liquid, the droplet spreads over the surface without phase change. In this heat transfer regime, the temperature at the interface (i.e. the contact temperature) determines the rate of heat exchange between the drop and the target. The most relevant temperature variations occur in the early instants after impact ($\tau - \tau_0 < 5$), where $\tau = t/D_0/U_0$ and are associated to the fast heat transfer occurring from the heated surface to the liquid, which is initially at room temperature. Therefore, the surface temperature decreases suddenly and then recovers at nearly T_{w0}, for later stages after impact. This behaviour is illustrated in Figure 1, which depicts the instantaneous temperature of a stainless steel surface during the impact of single droplets of different liquids.

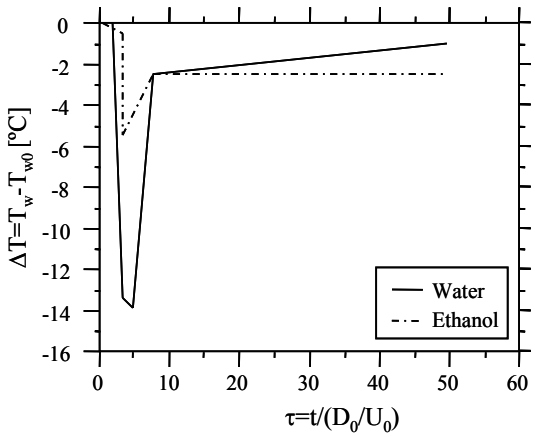

Figure 1. Instantaneous surface temperature, measured at the point impact of water (D_0=2.8mm, U_0=1.3ms^{-1}) and ethanol (D_0=2.4mm, U_0=1.3ms^{-1}) drops colliding on a stainless steel surface (R_a=0.31μm, R_z=2.32μm), within the single phase evaporation regime ($\Delta T=T_{sat}-T_{w0}$=15ºC).

The differences between the curves are mostly attributed to the distinct liquid properties (heat capacity and thermal conductivity) rather than to the impact conditions. Additionally, the much smaller surface tension of the ethanol and HFE7100 droplets (which also decreases with temperature at a larger slope) favours the occurrence of a number of morphological features in the lamella of these liquids (*e.g.* the formation of cellular structures due to surface temperature gradients) which will favour the fast evaporation and even disruption of the lamella, decreasing the contact area and residence time of the liquid over the surface. These particular features in the morphology of the lamella will further contribute to the difference observed in the measured instantaneous temperatures.

The predominant role of the liquid properties is even more evident in the nucleate boiling regime. Again, an associative effect of the liquid properties, particularly the liquid surface tension and the latent heat of evaporation will cause significant morphological differences in the lamellas of the various liquids, which contribute to the overall larger temperature decrease of the surface temperature when impacted by the water droplets, as shown in Figure 2. These morphological characteristics, previously discussed in Moita and Moreira [16] will promote the disruption of the lamella and the formation of dryout regions. Moreover, the associated effect of small σ_{lv} and h_{fg} will also favour the anticipation of the intense thermal induced atomization period, thus reducing the liquid mass that is cooling the surface (Moita and Moreira [16,22]).

The surface temperature does not recover to its initial value, particularly for liquids with larger h_{fg}. Small temperature oscillations (most of them smoothed in the final curves presented here) are actually associated to the coexistence of liquid and vapour phases in the measurement region, due to the intense bubble formation and growth within this regime.

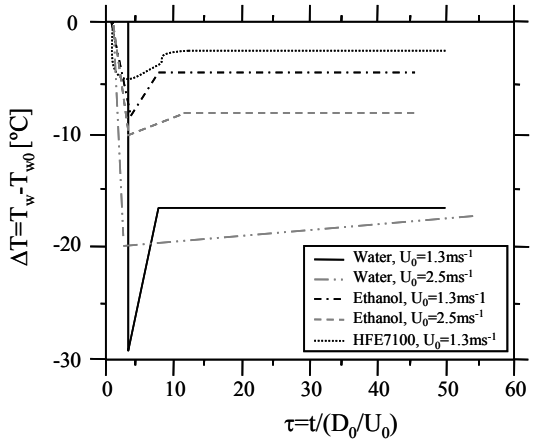

Figure 2. Instantaneous surface temperature, measured at the point impact of water (D_0=2.8mm), ethanol (D_0=2.4mm) and HFE7100 (D_0=2.0mm) droplets colliding on a stainless steel surface (R_a=0.31μm, R_z=2.32μm) at different velocities, within the nucleate boiling regime ($\Delta T=T_{w0}-T_{sat}$ =20ºC).

Figure 3 summarizes the effect of the impact velocity on temperature decay, for water and ethanol droplets. The figure includes the experimental data and numerical calculations of Pasandideh-Fard *et al.* [10] for water droplets impacting on a stainless steel surface.

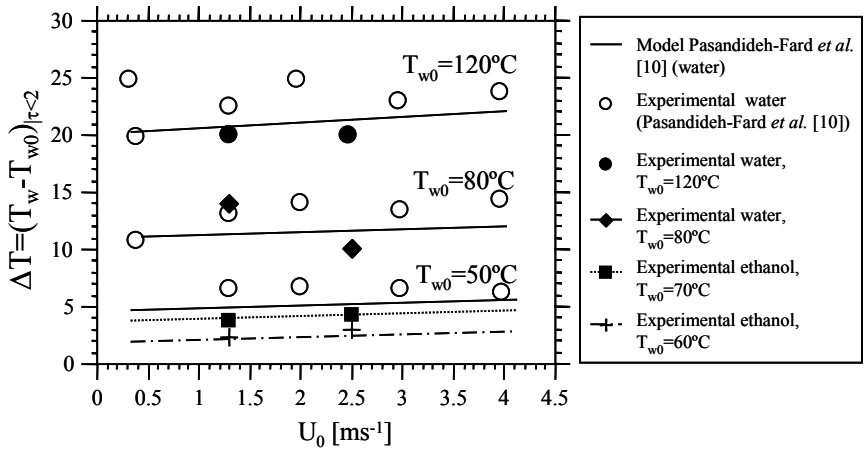

Figure 3. Effect of the impact velocity on the initial decay of instantaneous surface temperature, taken for $\tau<2$. The experimental results of the present paper are compared with both experimental results and numerical predictions reported in Pasandideh-Fard *et al.* [10].

Besides showing a good overall agreement between our data and the results of Pasandideh-Fard *et al.* [10], the figure clearly evidences the little effect of impact velocity on ΔT, when compared to the use of different liquids (*e.g.* ΔT for ethanol droplets at T_{w0}=60ºC is equivalent to that of water droplets impacting the surface that is initially much colder).

Further increasing the initial surface temperature, the nucleation mechanism is intensified leading to the formation of a vapour layer beneath the surface in the beginning of the onset of the CHF condition. As discussed in Moita and Moreira [16] and in Kandlikar *et al.* [23, 24] this mechanism can be explained by the formation of a dryout region due to the rapid evaporation of the lamella at the liquid-solid interface, which can occur due to a nucleation cavity or near the contact line region. In this case, the vapour pressure pushes the contact line, altering the contact angle so that a thin vapour layer moves underneath the lamella. Then, depending on the force balance in the contact line region, (in which the liquid surface tension has an imperative role) and on several mechanisms such as hydrodynamic effects (*e.g.* Marangoni effects), adhesion forces, or the surface temperature which may not be high enough, the liquid can re-wet the surface, thus delaying the establishment of the stable film boiling regime. Therefore, especial care must be taken when using liquids like HFE7100 in cooling systems, as they gather the properties (small σ_{lv} and small h_{fg}) which favour the formation of cellular structures, the disintegration of the lamella and the intense boiling and thermal induced atomization mechanisms, leading to dryout regions.

Up to this point, the analysis has been focused on the effect of the various governing parameters (liquid and surface properties and impact conditions) on the instantaneous surface temperatures. However it is also important to quantify the heat transferred between the droplet and the surface to understand how it is affected by the experimental conditions. In this context, total heat transfer from the surface to the droplet, for various impact conditions and liquids is depicted in Figure 4. The total heat transfer is considered here to take into account the effect of the wetted area.

The liquid properties are still the most relevant parameters affecting the heat transfer, so that the heat removed by the water droplets is significantly larger than that removed by the ethanol droplets (about 10times larger). The morphological modifications occurring within the lamella, which are associated to the properties of liquids like HFE7100 and ethanol (small k, small σ_{lv} and small h_{fg}), as discussed in the previous paragraphs are not taken into account in this evaluation, so that effective differences between the heat transferred by the water and by these liquids can be actually larger.

The impact velocity still plays a secondary role, although its effect is now more noticed since increasing impact velocity will enlarge the spreading area thus enhancing the heat transfer. This effect seems to be more pronounced for liquids which partially wet the surface, as the spreading phase occurs within a smaller time scale at which the inertial effects are more important, so increasing the impact velocity will affect substantially the spreading area. On the other hand, for liquids which completely wet the surface there is no recoiling phase, so the spreading occurs within a larger temporal scale, governed by capillary effects.

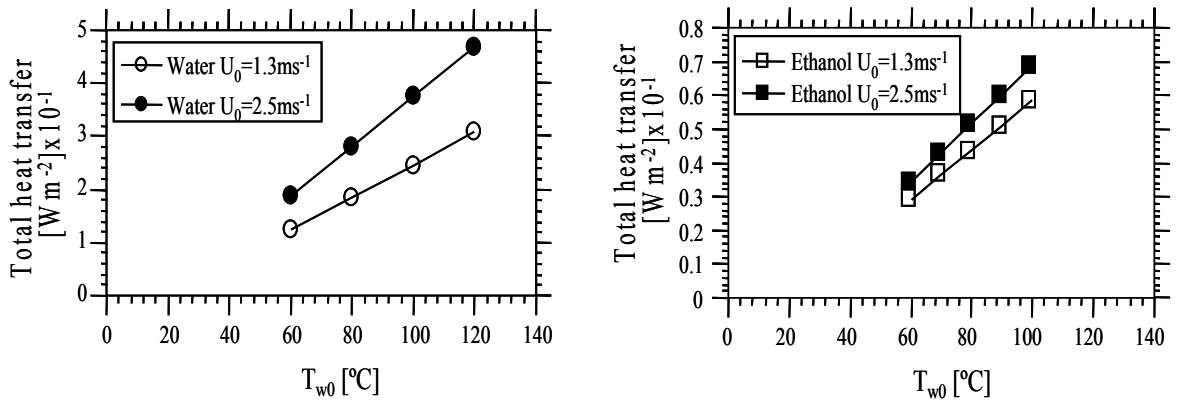

Figure 4. Total heat transferred between the impinging droplet and a smooth stainless steel surface (R_a=0.311μm, R_z=2.32μm); a) impact of water droplets (D_0=2.8mm) at different velocities, b) impact of ethanol (D_0=2.4mm) droplets at different velocities.

To conclude this analysis, one should also look at the parameters governing the cooling effectiveness of the impinging droplets, ξ. According to Pasandideh-Fard *et al.* [10] the cooling effectiveness may be defined as the ratio between the heat transferred between the spreading droplet and the surface with the maximum heat that the droplet can theoretically remove from the surface, i.e.:

$$\zeta = \frac{\int_0^t \int_0^A q'' dA dt}{mC_p(T_{w0} - T_{d0})} \tag{1}$$

being q'' is the heat flux from the surface and A the wetted area of the spreading lamella. T_{w0} and T_{d0} are the initial surface and droplet temperatures, respectively. The mass of the droplet m is determined by $m=\rho\,\pi/6D_0^3$.

The total heat transfer from the heated surface to the spreading drop can be estimated as:

$$q_c = \int_0^{t_c} \int_0^{A_{\max}} q'' dA dt \approx q'' A_{\max} t_c \tag{2}$$

where $A_{\max} = \pi D_{\max}^2 / 4$ is the maximum spreading area occurring at the corresponding instant t_c. The heat flux is given as:

$$q'' = k \frac{T_{w0} - T_{d0}}{\delta_T} \tag{3}$$

The thermal boundary layer thickness δ_T can be determined from a similarity solution for heat transfer for axisymetric stagnation point flow (White [25]):

$$\delta_T = \frac{\delta_u}{\mathrm{Pr}^{0.4}} \tag{4}$$

where δ_u is the hydrodynamic boundary layer thickness which, according to White [25] and following the scaling performed in Pasandideh-Fard *et al.* [26] can be estimated as:

$$\delta_u = 2D_0\,\mathrm{Re}^{-0.5} \tag{5}$$

Combining eqs. (4) and (5) one obtains:

$$\delta_T = 2D_0\,\mathrm{Re}^{-0.5}\,\mathrm{Pr}^{0.4} \tag{6}$$

Finally, introducing eq.(6) in eq.(3), the heat flux during the spreading of the lamella can be estimated as:

$$q'' = k \frac{T_{w0} - T_{d0}}{2D_0} \mathrm{Re}^{0.5} \mathrm{Pr}^{0.4} \tag{7}$$

In the present work δ_T and δ_u are estimated as in Pasandideh-Fard *et al.* [10] (numerical calculations show that this is a good approximation for the conditions studied here) and D_{max} is measured from the images taken by the high-speed cameras.

The most practical analysis allowing the future development of empirical correlations (which is the most common approach in these studies) should relate ξ with the influencing parameters in a dimensionless form. For an ease of analysis, at this stage of the study we will not consider the occurrence of liquid phase change. Following a dimensionless analysis, ξ can be well related with the Reynolds, the Weber and the Prandtl number. In this context, Figure 5 shows the theoretical relation between the cooling effectiveness, as determined by Pasandideh-Fard *et al.* [10] with the Weber, Reynolds and Prandtl numbers, compared with the cooling effectiveness determined from the present experimental results, for droplets of various liquids, impacting on a stainless steel surface. These results do not account for any reduction of liquid mass in contact with the contact area produced by droplet disintegration, since the impact velocities are low enough to prevent *prompt splash* and the surface temperature is not high enough to promote thermal induced atomization occurring during liquid boiling.

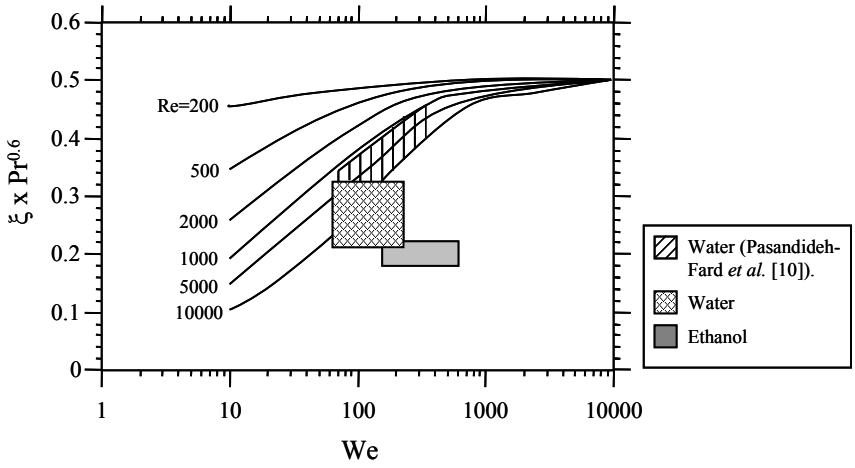

Figure 5. Cooling effectiveness ξ related with the Weber, the Reynolds and the Prandtl numbers, as in Pasandideh-Fard *et al.* [10].

The impact conditions indirectly influence the results, as they will alter the wetted area and therefore the heat that is removed from the surface. So, following the definition of ξ in eq.(1), the droplets impacting the surface with larger U_0 will have larger q_c and consequently slightly larger effectiveness. However the Figure clearly shows, consistently with the analysis performed so far, that the cooling performance of the water droplets is always larger than that of the ethanol droplets, for various impact velocities. The difference between the cooling effectiveness of the water and of the ethanol droplets is actually larger than that represented in Figure 5, since here ξ is already weighted with the Prandtl number of each liquid. This difference should also be more pronounced within the nucleate boiling regime given all the arguments related to the morphological aspects of the lamella and the characteristics of the thermal induced atomization discussed in the previous paragraphs. Quantifying these effects in the cooling effectiveness is a complex task, but vital to maximize the heat removal within the bubble boiling regime and take advantage of the additional parcel of the latent heat of evaporation. In this case, the associated effect of σ_{lv} and h_{fg} should be quantified introducing the Jakob number (Moita and Moreira [22]).

From these results we may also conclude that the cooling effectiveness of an impacting droplet within the single phase heat transfer regime can be well represented in the dimensionless space formed by the Prandtl-Weber numbers, as suggested by Pasandideh-Fard *et al.* [10], but not by the Reynolds number, particularly when the analysis includes other liquids besides water. This may suggest an alternative scaling of the parameters, where more weight should be given to the surface tension forces in destabilizing the shape of the lamella and to the Prandtl number giving the relation between the thickness of the thermal and hydrodynamic boundary layers. However, a further investigation is still required until we can achieve a final form for such relation.

Conclusions

The present paper identifies the effect of the various parameters influencing the heat transfer mechanisms occurring at the liquid-solid interface during droplet impact onto a hot rigid surface. The numerous experiments, performed in an extensive study, address the impact of droplet of various liquids, within a wide range of impact conditions, covering all the heat transfer mechanisms. The analysis performed here reinforces the major role of the liquid properties when compared to that of the impact conditions and suggests that the cooling effectiveness of impacting droplets can be well represented in the dimensionless space Prandtl-Weber number, within the single phase heat transfer regime.

Acknowledgements

The authors acknowledge the contribution of the National Foundation of Science and Technology by supporting A.S. Moita with a Fellowship (REF:SFRH/BPD/63788/2009) and by partially financing the research through the project PTDC/EME-MFE/69459/2006.

Nomenclature

A	spreading area [m^2]
C_p	specific heat [$kJkg^{-1}K^{-1}$]
D	droplet diameter [mm]
m	mass [kg]
h_{fg}	latent heat of evaporation [$kJkg^{-1}$]
Ja	Jakob number($= C_p(T_w - T_{sat})/h_{fg}$)
k	thermal conductivity [$Wm^{-1}K^{-1}$]
Pr	Prandtl number ($=\nu C_p \rho / k$)
R_a	mean surface roughness [μm]
R_z	mean peak-to valley roughness [μm]
Re	Reynolds number ($=U_0D_0/\nu$)
T	temperature [ºC]
t	time [s]
U	velocity component normal to the surface [ms^{-1}]
We	Weber number ($= \rho D_0 U_0^2 / \sigma_{lv}$)
τ	dimensionless time ($=t/(D_0/U_0)$)
ΔT	temperature difference [ºC]
ε	thermal effusivity ($=(\rho k C_p)^{1/2}$) [$W^{-1}s^{1/2}/m^2K$]
ν	kinematic viscosity [m^2s^{-1}]
θ	static contact angle [º]
ρ	specific mass [kgm^{-3}]
σ_{lv}	surface tension of the liquid [Nm^{-1}]
ξ	cooling effectiveness

Subscripts

0	initial (t=0s)
c	contact
CHF	Critical Heat Flux
d	droplet
max	maximum
sat	saturation
w	wall

References

[1] Amon, C.H., Yao, S.-C., Hsieh, C.-C., *Transactions of the ASME* 127:66-75 (2005).
[2] Shedd, T.A., *Heat Transf. Eng.* 28:87-92 (2007).
[3] Fest, S., Schmidt, J., *11th Triennial International Conference on Liquid Atomization and Spray Systems, ICLASS 2009*, Vail, Colorado, USA, July 2009.
[4] Paik, P.Y., Chakrabarty, K., Pamula, V.K., "Adaptive cooling of integrated circuits using digital microfluidics", *Artech House* (2007).
[5] Royne, A., Dey, C.J., Mills, D.R., *Solar Energy Mat. & Solar Cells* 86:451-483 (2005).

[6] Panão, M.R.O, Moreira, A.L.N., *Int. J. Heat Fluid Flow* 30:117-130 (2007).
[7] Tartarini, P., Corticelli, M.A., Santangelo, P.E., *11th Triennial International Conference on Liquid Atomization and Spray Systems, ICLASS 2009*, Vail, Colorado, USA, July 2009.
[8] Labeish, V.G., *Exp. Thermal Fluid Sci.* 8:181-184 (1994).
[9] Chen, J.C., Hsu, K.K., *J., Heat Transf.* 117:693-697 (1995).
[10]Pasandideh-Fard, M., Aziz, S.D., Chandra, S., Mostaghimi, J., *Int. J. H. Fluid Flow* 22:201-210 (2001).
[11]Healy, W.M., Hartley, J.G., Abel-Khalik, S.I., *Int. J. H. Mass Transf.* 44:3869-3881 (2001).
[12]Sawyer, M.L., Jeter, S.M., Abdel-Khalik, S.I., *Int. J. Heat Mass Transf.* 40(9):2123-2131 (1997).
[13]Incropera, F.P., DeWitt, D.P., "Fundamentals of Heat and Mass Transfer", 3rd Ed., *John Wiley & Sons*, 1990.
[14]Özisik , M.N., "Heat Transfer: a Basic Approach", *Mc-Graw Hill*, 1985.
[15]Turns, S.R., "An Introduction to Combustion: Concepts and Applications", *McGraw-Hill*, 1996.
[16]Moita, A.S., Moreira, A.L.N., *23rd Annual Conference on Liquid Atomization and Spray Systems, ILASS 2008*, Como Lake, Italy, September 2008.
[17]Tamura, Z., Tanasawa, Y., *7th Symp. (Int.) Combustion*, Buttertvorths, London, England (1959).
[18]Qiao Y.M., Chandra, S., *Proc. Royal Soc. London A* 453:673-689 (1997).
[19]Seki, M, Kawamura, H., Sanokawa, K., *J. Heat Transf.* 100:167-169 (1978).
[20]Nunes de Carvalho, C., Lavareda, G., Parreira, P. Amaral, A. Botelho do Rego, A.M., *J. Non-Crystalline Solids* 354:1643-1647 (2007).
[21]Moita, A.S., Moreira, A.L.N., *Int. J. Heat Fluid Flow* 28:735-752 (2007).
[22]Moita, A. S., Moreira, A. L. N., *Exp. Fluids* 47:755-768 (2009).
[23]S. G. Kandlikar, S.G., Steinke, M.E., *Int. J. Heat Mass Transf.* 45:3771-3780 (2002).
[24]Kandlikar, S.G., *ASME J. Heat Transfer* 123:1071-1079 (2001).
[25]White, F.M., "Viscous fluid flow", 2nd Ed., *McGraw-Hill*, 1991.
[26]Pasandideh-Fard, M., Bhola, R., Chandra, S., Mostaghimi, J., *Phys. Fluids* 8:650-659 (1996).